ACS APPLIED ENERGY MATERIALS

Article

Cite This: ACS Appl. Energy Mater. 2018, 1, 475−482

www.acsaem.org

CdS/Low-Band-Gap Kesterite Thin-Film Solar Cell Absorber Heterojunction: Energy Level Alignment and Dominant Recombination Process

Marcus Bär,[*,†,‡] Thomas Schnabel,[§] Jan-Hendrik Alsmeier,[†] Stefan Krause,[†,∥] Norbert Koch,[†,∥] Regan G. Wilks,[†,‡] and Erik Ahlswede[§]

[†]Renewable Energy, Helmholtz-Zentrum Berlin für Materialien und Energie GmbH (HZB), Hahn-Meitner-Platz 1, 14109 Berlin, Germany

[‡]Energy Materials In-situ Laboratory Berlin (EMIL), Helmholtz-Zentrum Berlin für Materialien und Energie GmbH, Albert-Einstein-Straße 15, 12489 Berlin, Germany

[§]Zentrum für Sonnenenergie- und Wasserstoff-Forschung Baden-Württemberg (ZSW), Meitnerstraße 1, 70563 Stuttgart, Germany

[∥]Institut für Physik, Humboldt-Universität zu Berlin, Newtonstraße 15, 12489 Berlin, Germany

Supporting Information

ABSTRACT: The chemical and electronic interface structure (including energy level alignment) between wet-chemical deposited CdS and low-band-gap $Cu_2ZnSn(S,Se)_4$ (CZTSSe) thin-film solar cell absorbers was studied using direct and inverse photoemission. Complementarily, the activation energy (E_a) of the dominant charge carrier recombination process of related solar cell devices was derived by temperature-dependent current−voltage [$I(V,T)$] measurements. We find the CZTSSe surface to be free of any significant amount of sulfur and the formation of Cd−Se bonds at the interface. A small, positive ("spike"-like) conduction band offset of 0.21 ± 0.28 eV between CZTSSe and CdS was measured. In conjunction with the $I(V,T)$ derived E_a of 1.09 ± 0.07 eV, which is in excellent agreement with the CZTSSe bulk band-gap energy of 1.07 eV, this reveals that high-rate charge carrier recombination at the CdS/CZTSSe interface can mainly be excluded as the performance-limiting factor in corresponding solar cells.

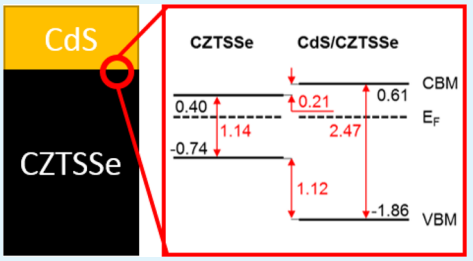

KEYWORDS: *thin-film solar cell, kesterite, energy level alignment, dominant recombination process, photoemission*

INTRODUCTION

Thin-film solar cell absorbers based on the earth-abundant $Cu_2ZnSn(S,Se)_4$ (CZTSSe) kesterite material system have attracted much attention in the past (see refs 1−4 for comprehensive reviews on the past developments, the current state-of-the-art, and future challenges). The optoelectronic properties can easily be tuned resulting in optical band-gap energies (E_g) between around 1.0 eV[5,6] for the pure selenides [$Cu_2ZnSnSe_4$ (CZTSe)] and 1.5 eV[5−7] for the pure sulfides [Cu_2ZnSnS_4 (CZTS)]. On a laboratory scale, power conversion efficiencies of up to 12.6%[8] for solar cells based on low bulk band-gap (E_g = 1.13 eV) mixed S/Se kesterites have been reached. In recent years, the progress in device performance somehow fell back compared to the expectations created by the fast improvements in the early development phase.[9] A significant open circuit voltage (V_{OC}) deficit, i.e., a particularly large difference between $E_{g,CZTSSe}$ of the kesterite absorber material and V_{OC} of the corresponding solar cell, was identified as being the main culprit for this shortage.[1,10] High-rate charge carrier recombination at the (defect-rich) buffer/absorber interface—due to an unfavorable energy level alignment—has been discussed as one possible underlying mechanism for this deficiency.[1,3,4,10] Indeed, detailed device characterization of CdS/CZTSSe[1,11,12] and CdS/CZTS[1,13−15] solar cells reveal that the activation energy of the dominant recombination process (E_a) is generally smaller than $E_{g,CZTSSe}$. This is commonly interpreted as an indication for a recombination at the buffer/absorber interface.[16,17] However, note that, for CZTSe,[11] for low-band-gap (i.e., $E_{g,CZTSSe} \leq 1.2$ eV) CZTSSe[18] absorbers, and for $Zn_{1-x}Sn_xO_y$/CZTS structures,[14] a few studies also report E_a values that do correspond to $E_{g,CZTSSe}$, which would rather be in agreement with the dominant recombination mechanism being located in the (comparably defect-poor) absorber bulk. The photogenerated electrons have to pass the CdS/CZTSSe interface, so the conduction band (CB) alignment at this interface is crucial for determining the recombination path. One possible explanation for interface-limited devices would be a (negative) "cliff"-like CB offset (CBO) at the CdS/kesterite interface, in which the CB minimum (CBM) of the CdS buffer lies below that of the

Received: November 2, 2017
Accepted: February 1, 2018
Published: February 1, 2018

DOI: 10.1021/acsaem.7b00071
ACS Appl. Energy Mater. 2018, 1, 475−482

kesterite absorber. As pointed out by Scheer,[17] this alignment would result in a reduction of the interface band gap ($E_{g,i}$), which is the sum of the absorber surface band-gap and the CBO: $E_{g,CZTSSe}^{surf}$ + CBO, presenting the energetic barrier for a charge carrier recombination path across the interface. In contrast, an aligned or slightly (positive) "spike"-like CBO (i.e., where the CdS CBM lies above that of the kesterite absorber) would be considered an ideal energy level alignment for efficient charge carrier transport at the buffer/absorber interface in a kesterite-based solar cell, as it establishes the full energetic barrier preventing interfacial charge carrier recombination while not impeding electron transport.[19]

In order to clarify the electronic structure of the interface between wet-chemically deposited CdS (i.e., the standard buffer layer in kesterite-based devices) and low-band-gap CZTSSe absorbers and how it relates to the dominant recombination mechanism in respective solar cells, a combined spectroscopic and device study has been performed. In detail, we have used direct and inverse photoemission to independently measure the position of the valence band maximum (VBM) and the CBM and, thus, also the electronic surface band gap (E_g^{surf}) of the buffer and the absorber. Together with the information on interface-induced band bending—derived from studying a CdS thickness series on CZTSSe—this insight allows one to reveal the valence band offset (VBO) and the CBO at the CdS/CZTSSe interface using a purely experimental approach. This energy level alignment picture is complemented by the determination of the activation energy of the dominant recombination process by temperature-dependent current−voltage [$I(V,T)$] measurements of related solar cells. We find that—at the current state and for the studied material—the CdS/(low-band-gap) CZTSSe interface does not limit the device performance.

EXPERIMENTAL SECTION

The investigated layers and devices were prepared at ZSW and sent to HZB for characterization. The polycrystalline CZTSSe thin films (approximately 1 μm thick) were deposited on Mo-coated soda-lime glass using a metal salt solution of copper(II) acetate monohydrate, zinc(II) chloride, tin(II) chloride, and thiourea in dimethyl sulfoxide. Afterward the CZTS precursor layer was annealed in Se atmosphere at a temperature of 550 °C in a tube furnace. This process of (partially) selenizing a S-containing precursor film at elevated temperature results in a final composition of S/(S + Se) ≈ 0.1 in the bulk of the CZTSSe absorber.[20] X-ray fluorescence (XRF) analysis of the absorber material under study further reveals an intentionally Zn-rich and Cu-poor bulk composition of Zn/Sn = 1.16 and Cu/(Zn + Sn) = 0.76, which deviates from the nominal bulk composition of Zn/Sn = 1 and Cu/(Zn + Sn) = 1 but is in general agreement with the composition found for high-performing kesterite absorbers.[20] The bulk band gap of these CZTSSe absorbers as derived by external quantum efficiency measurements is 1.07 eV.[20]

A CdS thickness series was prepared on the CZTSSe absorbers in a chemical bath (of cadmium sulfate, thiourea, and aqueous ammonia) at 60 °C using deposition times of 1 s and 1, 2, 3, and 4 min. A deposition time of 8 min is generally used for buffer layers in respective solar cell devices resulting in a CdS thickness of approximately 50 nm. Half of the thickness series samples was used to prepare solar cells by adding a sputtered ZnO window layer and a ZnO:Al front contact. Figure S1 [see Supporting Information (SI)] shows the current−voltage curve and external quantum efficiency data of a representative solar cell for the 4 min CdS/CZTSSe layer stack, and Table 1 shows the respective solar cell parameters for all devices. It can be observed that with increasing CdS deposition time (i.e., buffer layer thickness) all the device parameters improve up to 3 min CBD time, reaching a maximum power conversion efficiency of 5.5%.

Table 1. Average Photovoltaic Parameters [Power Conversion Efficiency (η), Open Circuit Voltage (V_{OC}), Short Circuit Current (I_{SC}), and Fill Factor (FF)] of the Solar Cells Prepared from the Studied CdS/CZTSSe Thickness Series Samples (Measured under Standard Test Conditions: AM 1.5, 100 mW/cm^2, and 25°C)[a]

deposn time	estd thickness (nm)	η (%)	V_{OC} (mV)	I_{SC} (mA)	FF (%)	E_a (eV)
0	0	0	0	0	0	N/A
1 s	0	0	83	0.1	23	N/A
1 min	1	0.8	297	13	21	N/A
2 min	3	2.8	368	25	31	N/A
3 min	5	5.5	376	29	51	N/A
4 min	20	4.7	403	26	43	1.09

[a]For the 4 min CdS/CZTSSe-based solar cell also the activation energy of the dominant recombination process (E_a) derived from $I(V,T)$ measurements is given. The stated thicknesses are estimates based on the fact that a 8 min CBD-CdS layer results into a 50 nm thick buffer and considering that there is a significant induction period (i.e., a period in which no deposition takes place) at the beginning of the CBD process.

For the 4 min sample—despite the highest open circuit voltage—the efficiency is lower due to a decrease in the short circuit current and fill factor, presumably caused by a too thick CdS layer that may result in too much absorption in the UV and/or a too high series resistance. Note that optimized devices based on these CZTSSe absorbers are able to reach efficiencies of up to 10.3% power conversion efficiency.[21]

Right after CBD-CdS deposition the samples were immediately sealed under inert gas (air exposure was limited to <1 min) and send to HZB for characterization.

The samples were transferred via a N_2-purged glovebox/glovebag into the ultrahigh-vacuum (UHV; base pressure < 5 × 10^{-10} mbar) surface analysis system for X-ray (XPS), ultraviolet (UPS) photoelectron, and X-ray excited Auger electron (XAES) spectroscopy as well as inverse photoemission (IPES). For XPS, XAES [UPS] nonmonochromatized Mg Kα [He I] excitation and a Specs PHOIBOS 150 MCD electron analyzer (calibrated according to ref 22) were used. For IPES, a commercial PSP Vacuum Technology setup consisting of a low-energy electron gun and a solid-state photon detector was used. The electron gun used a cathode with a BaO dispenser resulting in a sample current of 5−10 μA. The detector consists of a photon energy bandpass filter (i.e., fluoride window in combination with a NaCl-coated Ta cone) and an electron multiplier. For a common UPS and IPES energy scale, the Fermi level (E_F) of a gold foil was used. For all measurements, the top surface of the samples was short circuited to the Mo layer and grounded. For sample cleaning, a mild ion treatment using 100 eV Ar^+ ions was used.

$I(V,T)$ measurements were performed using a Keithley 2400 source measuring unit under simulated AM 1.5 global solar irradiation with a WACOM 2-lamp sun simulator at 100 mW cm^{-2}. The temperature was varied between 282 and 339 K, which is the maximum temperature range of the employed setup. External quantum efficiency measurements to determine the bulk band gap were performed with a setup from Optosolar.

RESULTS AND DISCUSSION

Figure 1 shows the survey spectra of the studied CdS/CZTSSe samples series. All prominent buffer (Cd MNN, Cd 3d, and S 2p) and absorber (Zn 2p, Cu 2p, Sn MNN, Sn 3d, Cu LMM, Zn LMM, S 2p, and Se 3d) related XPS and XAES peaks can be observed. With increasing CBD time, the buffer related lines increase while the absorber peaks are attenuated, as expected. There is no indication for a CBD-induced interfacial intermixing involving zinc, copper, and/or tin (see Figure S2

DOI: 10.1021/acsaem.7b00071
ACS Appl. Energy Mater. 2018, 1, 475−482

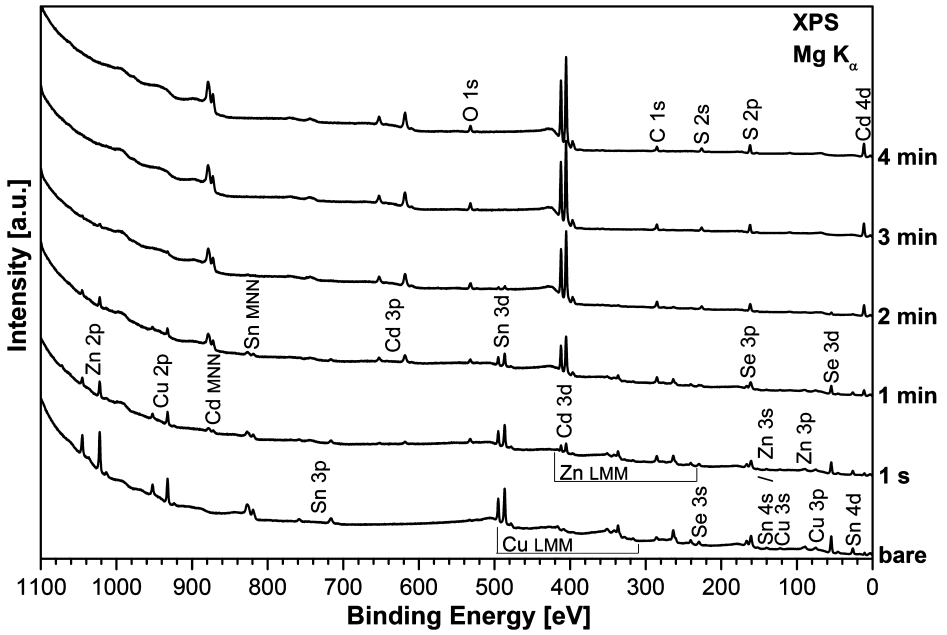

Figure 1. XPS survey spectra of the bare CZTSSe absorber and the buffer/absorber samples of the CdS thickness series. The CdS deposition time is given at the right. The most prominent XPS and XAES lines are labeled, and the spectra have been offset for clarity.

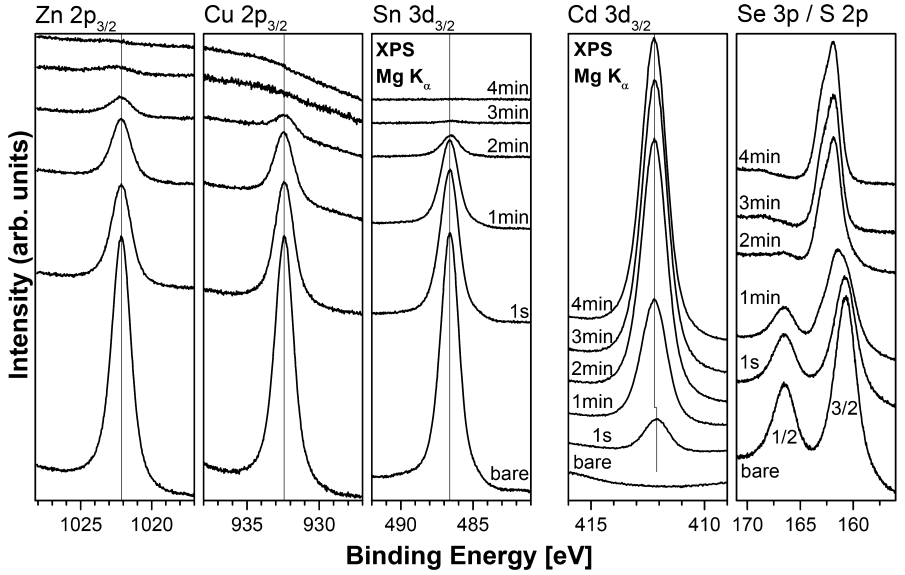

Figure 2. XPS Zn 2p$_{3/2}$, Cu 2p$_{3/2}$, Sn 3d$_{3/2}$, Cd 3d$_{3/2}$, and Se 3p/S 2p detail spectra of the bare CZTSSe absorber and the buffer/absorber samples of the CdS thickness series. The spectra are identified at the top, and the CdS deposition times are indicated. The spectra have been offset for clarity.

and related discussion for details), in contrast to our recent finding of a distinct elemental "redistribution" at the CdS/CZTSe interface involving formation of a Zn−Se−Cd−S interlayer, which we attributed to ion exchange mediated by the amine complexes present in the chemical bath.[23] An explanation for this difference could be the deliberate Zn termination of the CZTSe kesterite—and thus the presence of ZnSe at the absorber surface—in our previous study. In addition to the expected XPS and XAES signals, oxygen and carbon related signals can be observed. Both the O 1s and C 1s lines show increased intensity after CBD compared to the spectrum of the bare CZTSSe absorber, which suggests that to some degree oxygen and carbon are incorporated into the buffer layer. However, the presence of an O- and C-containing surface contamination layer cannot be excluded.

In Figure 2 the detailed XPS spectra of the most prominent absorber (Zn 2p$_{3/2}$, Cu 2p$_{3/2}$, Sn 3d$_{3/2}$, Se 3p, and S 2p) and buffer (Cd 3d$_{3/2}$ and S 2p) related photoemission lines are depicted. Note that for the Sn 3d and Cd 3d, we show the 3d$_{3/2}$ instead of the more intense 3d$_{5/2}$ spectrum to avoid the overlap with the Mg K$\alpha_{3,4}$ excited satellites of the 3d$_{3/2}$ line. Again, a decrease of the absorber peaks and an increase of the buffer signals can be observed with increasing CBD time due to the thicker growing buffer layer. For a CBD time of 4 min, all the absorber peaks disappear completely indicating that a buffer layer with a *minimum* thickness of approximately 5 nm (=3 × inelastic mean free path [IMFP] of the Sn 3d$_{3/2}$ photoelectrons in CdS[24]) completely covers the kesterite absorber. Neither the spectral shape nor the binding energy position of the Zn 2p$_{3/2}$, Cu 2p$_{3/2}$, and Sn 3d$_{3/2}$ lines change (see three leftmost panels

DOI: 10.1021/acsaem.7b00071
ACS Appl. Energy Mater. 2018, 1, 475−482

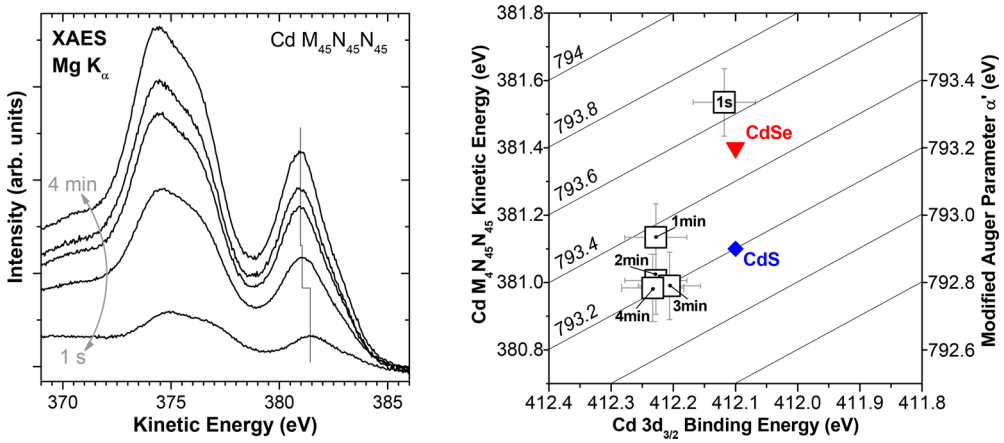

Figure 3. Left: Cd $N_{45}N_{45}N_{45}$ XAES detail spectra of the buffer/absorber samples of the CdS thickness series. The CdS deposition times are indicated by the arrow. Right: Wagner plot of the modified Auger parameter for the CdS thickness series samples. For comparison also the modified Auger parameter for CdS and CdSe [data from ref 31] are indicated.

in Figure 2), pointing to formation of an "abrupt" interface—at least from the absorber's perspective—without significant chemical interaction and/or a *change* in band bending induced by the formation of the CdS/CZTSSe interface. The fact that the absorber core levels do not shift toward higher binding energies with CdS deposition (which would indicate a downward band bending as expected for the energy levels of a p-type semiconductor when brought into direct contact with an n-type material) points to Fermi level pinning presumably due to a high density of defects at the absorber surface and/or buffer/absorber interface. However, note that a preexisting downward band bending at the CZTSSe surface (caused by the same defects) cannot be excluded and is corroborated by the UPS/IPES results discussed below.

Taking the respective values for IMFP,[24−26] photoionization cross-section,[27] and transmission function of the electron analyzer into account, the Zn $2p_{3/2}$, Cu $2p_{3/2}$, and Sn $3d_{3/2}$ line intensities can be used to derive surface composition information. We find the CZTSSe absorber surface to be significantly Zn-rich (Zn/Sn ≈ 1.4) and Cu-poor [Cu/(Zn + Sn) ≈ 0.5] with respect to the XRF-derived bulk composition (Zn/Sn = 1.16 and Cu/(Zn + Sn) = 0.76) in agreement with previous studies.[23,28] Note that the deviation from the nominal bulk composition of Zn/Sn = 1 and Cu/(Zn + Sn) = 1 is even more pronounced. The quantification of the relative chalcogen contribution is complicated by the overlap of the S 2p and Se 3p signals. For the bare CZTSSe absorber, the respective spectral range is dominated by the $3p_{1/2}$ and $3p_{3/2}$ selenium signal separated by 5.7 eV[29] (see rightmost panel of Figure 2). As a matter of fact, there is no indication that any sulfur is present at the surface of the absorber—at least within the S/(S + Se) XPS detection limit, which is estimated to be in our case in the range of 0.01 (see SI Figure S3 for a more detailed discussion). By contrast, the CZTSSe absorber bulk has a sulfur content of S/(S + Se) ≈ 0.1.[20] Thus, we will continue to refer to this material as CZTSSe in the following. With increasing CBD time, the S 2p signal (the $2p_{1/2}$ and $2p_{3/2}$ doublet separation is only 1.2 eV[29] and hence the individual components cannot be completely resolved) appears between the Se $3p_{1/2}$ and $3p_{3/2}$ lines, completely dominating the spectrum for long CBD times (i.e., 2−4 min) as expected from the growing thickness of the CdS buffer.

The spectral shapes of the Cd $3d_{3/2}$ lines also do not change (see second from right panel of Figure 2); however, for the shortest CBD time a small shift to lower binding energies can be observed. To investigate whether this is due to a chemical shift or due to a change in band bending upon interface formation, the Cd $M_{45}N_{45}N_{45}$ XAES data are inspected (see Figure 3, left panel). The Cd $M_{45}N_{45}N_{45}$ spectrum increases in intensity with increasing CBD time, as expected and discussed above. Similarly to the Cd $3d_{3/2}$ line, also for the Auger spectra a similar spectral shape is observed and a shift to higher kinetic energies for short (i.e., 1 s and 1 min) deposition times, as indicated by the vertical line indicating the kinetic energy position of the Cd $M_4N_{45}N_{45}$ transition. In order to exclude changes in band bending, charging, and/or doping concentration as the underlying explanation for the shifts in the Cd 3d and Cd Cd $M_{45}N_{45}N_{45}$ signals, we consult the modified Auger parameter α_{Cd}* = binding energy (Cd $3d_{3/2}$) + kinetic energy (Cd $M_4N_{45}N_{45}$). In the right panel of Figure 3, the computed α_{Cd}* values for the whole data set are shown in a Wagner plot[30] in which the same values for α_{Cd}* can be found along the indicated diagonal lines. For comparison also the α_{Cd}* values for CdS and CdSe reference compounds[31] are indicated. To derive the latter values, the $3d_{3/2}$−$3d_{5/2}$ doublet separation of 6.8 eV[29] was added to the Cd $3d_{5/2}$ binding energies reported for CdS and CdSe. For long CBD times (2−4 min), the derived modified Auger parameters are very close together and agree with that of CdS α_{Cd}* (CdS) = 793.2 eV. For the 1 s CdS/CZTSSe sample—as a result of the lower Cd $3d_{3/2}$ binding energy and higher Cd $M_4N_{45}N_{45}$ kinetic energy discussed in conjunction with Figure 2 and the left panel of Figure 3—a significantly different α_{Cd}* of ≈793.6 eV is found, which is very close to the reported modified Auger parameter for CdSe (α_{Cd}* (CdSe) = 793.5 eV). For the intermediate 1 min CdS/CTSSe sample, a α_{Cd}* value is computed that lies close to those found for the longer deposition times but still somewhat between that of CdS and CdSe. From this we conclude that in the very first stages of the chemical bath process (i.e., the so-called induction period during which no sulfur is released from the thiourea) Cd−Se bonds are formed at the surface of the CZTSSe absorber, before—starting from a CBD time of 1 min—CdS is deposited. Taking the absorber core level line intensities of the bare CZTSSe (I_0) and of the 1 s CdS/CZTSSe (I) sample into account (see respective spectra in the three leftmost panels in

DOI: 10.1021/acsaem.7b00071
ACS Appl. Energy Mater. 2018, 1, 475−482

Figure 2) and assuming that they get attenuated by a homogeneous, completely covering CdSe layer, then this interfacial region can be estimated to be approximately 1 nm [=−IMFP $\ln(I/I_0)$] in dimension. (Note that the IMFP of CdSe was calculated according to refs 24−26.) The formation of interfacial Cd−Se bonds has been previously reported to occur on $CuGaSe_2$ absorbers upon treatment in a Cd^{2+}-ion-containing partial electrolyte treatment (simulating chemical bath conditions without sulfur source).[32] Note that the modified Auger parameters of CdO (α_{Cd}* (CdO) = 794.2 eV[31]) and/or $Cd(OH)_2$ (α_{Cd}* ($Cd(OH)_2$) = 791.7−791.9 eV[29]) are outside of the α_{Cd}* energy window depicted in the right panel of Figure 3, and hence it can be excluded that significant amounts of these compounds are present in the buffer layer. However, the presence of significant amounts of oxygen and carbon (see discussion in conjunction with Figure 1 above) could be explained by the formation of cadmium carbonate as suggested by Kylner et al.[33] Unfortunately, no Cd $M_{45}N_{45}N_{45}$ Auger data for $CdCO_3$ are reported in literature (and thus no modified Auger parameter can be computed). However, ref 29 states for the Cd $3d_{5/2}$ photoemission line a binding energy of 405.1 eV (which relates—assuming a doublet separation of 6.8 eV[29]—to a Cd $3d_{3/2}$ binding energy of 411.9 eV), which is in the range of the Cd 3d binding energy values found for the sample series under investigation (in particular when taking the spread for other Cd compounds listed in ref 29 into account—e.g., for CdO—the standard deviation of the reported Cd 3d reference binding energies is ±0.3 eV).

In order to gain insight into the electronic interface structure, additional UPS and IPES measurements were performed on the bare CZTSSe absorber and the 4 min CdS/CZTSSe sample. The respective spectra are shown in Figure 4. The left (right) side shows the UPS (IPES) spectra, and the top (bottom) spectra stem from the absorber (buffer/absorber) sample. For each measurement two spectra are shown, one of the as-received sample (gray line) and one of the sample that has been cleaned by a mild (100 eV) Ar^+- ion treatment (40 min for the CZTSSe and 45 min for the CdS/CZTSSe sample, black spheres). Due to the cleaning, the spectral features close to the Fermi level (E_F) become more pronounced and the spectral onsets generally move closer together. XPS data (not shown) show the removal of oxygen and carbon from the sample, which is in agreement with the presence of a surface contamination layer discussed above and its (partial) Ar^+-ion treatment-induced removal. The positions of the valence band maximum (VBM) and conduction band minimum (CBM) are derived by linear approximation of the leading spectral edge as indicated by the red lines in Figure 4. For the bare CZTSSe absorber [CdS/CZTSSe sample], we find the VBM to be at −0.74 ± 0.10 eV (−1.86 ± 0.10 eV) and the CBM at 0.40 ± 0.20 eV (0.61 ± 0.20 eV). Thus, the electronic surface band gap (E_g^{surf} = CBM − VBM) results in 1.14 ± 0.22 and 2.47 ± 0.22 eV for the absorber and the buffer/absorber samples, respectively. The latter is in accordance with optical bulk band-gap energies reported for CdS thin films deposited in a chemical bath.[34] The E_g^{surf} value for the CZTSSe absorber is—within experimental uncertainty—in agreement with the CZTSSe bulk band gap of 1.07 eV as derived by external quantum efficiency measurements.[20] However, note that depending on whether ordered or disordered kesterite is considered, an increase in $E_{g,CZTSSe}$ of approximately 0.05 or 0.08 eV, respectively, is reported for samples with their Cu/(Zn + Sn) composition decreasing from approximately 0.84 to 0.64.[35] Taking into account that we find the surface of the here studied CZTSSe absorber to be significantly Cu-poor [Cu/(Zn + Sn) ≈ 0.5, see above] compared to its bulk composition [Cu/(Zn + Sn) = 0.76], an $E_{g,CZTSSe}^{surf}$ value (1.14 eV) that is higher than the bulk band gap (1.07 eV) is in agreement with the identified surface Cu deficiency. In addition, the presence of sulfur (even in amounts below the XPS detection limit) would also result in an E_g increase. The fact that the Fermi level is located closer to the CBM (than to the VBM, as expected for a p-type semiconductor) might indicate a downward band bending at the bare absorber surface.

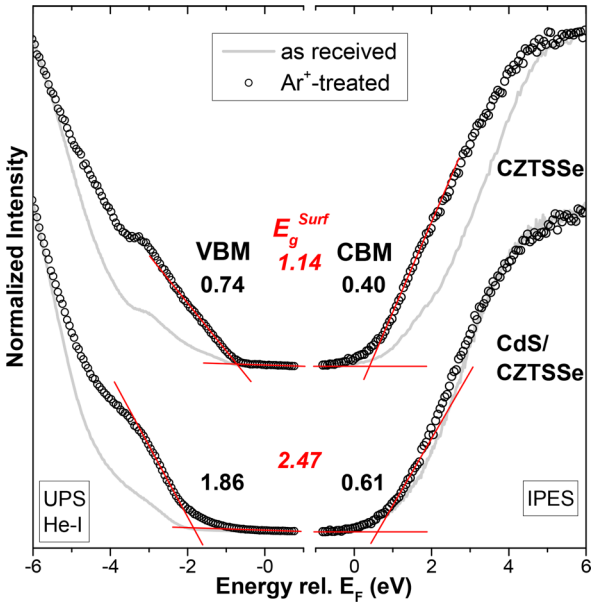

Figure 4. UPS (left) and IPES (right) spectra of the bare (top) and 4 min CdS/CZTSSe (bottom) spectra on a common energy scale relative to the Fermi level, E_F. The gray lines (black spheres) show the spectra of the as-received (Ar^+-ion treated/cleaned) samples, and the red lines indicate the linear extrapolations of the leading edges to derive the VBM and CBM positions. The resulting surface band gap, E_g^{surf}, is also given. All numbers are given in electronvolts. The experimental uncertainties for the VBM, CBM, and E_g^{surf} values are ±0.1, ±0.2, and ±0.22 eV, respectively.

To get insight into the energy level alignment at the CdS/CZTSSe interface, i.e., the valence band offset (VBO) and conduction band offset (CBO), the derived VBM and CBM values have to be compared. Both the VBM and CBM of the CdS/CZTSSe sample are further away from E_F than the values for the bare CZTSSe. As a result, the VBO can be computed to be +1.12 ± 0.14 eV and a CBO of +0.21 ± 0.28 eV is found, i.e., in the VB as well as in the CB so-called "spike"-like band discontinuities form at the CdS/CZTSSe interface. In Figure 5 a schematic presentation of the energy level alignment at the CdS/CZTSSe interface is depicted. Note that no correction for a change in band bending induced by interface formation has to be applied as neither the absorber nor the buffer core levels showed any related shift with increasing CBD time (see discussion in conjunction with Figure 2, above). The slight shift that has been observed in the Cd core level and Auger lines was attributed to a variation in the chemical environment at the interface. The suggested formation of interfacial Cd−Se bonds have, however, to be taken into account when discussing the energy level alignment at the CdS/CZTSSe interface. Based on

DOI: 10.1021/acsaem.7b00071
ACS Appl. Energy Mater. 2018, 1, 475−482

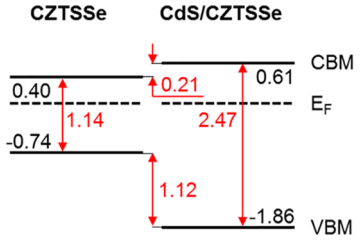

Figure 5. Schematic presentation of the VBM and CBM positions and resulting E_g^{surf} values at the surface of the bare CZTSSe and 4 min CdS/CZTSSe samples. All numbers are given in electronvolts. The experimental uncertainties for the VBM, CBM, and E_g^{surf} values are ±0.1, ±0.2, and ±0.22 eV, respectively. Since no significant interface-induced band bending was observed, this scheme also indicates the energy level alignment at the CdS/CZTSSe interface.

experimental[36] and theoretical[37] studies, both the VBM as well as the CBM move closer to E_F when comparing CdSe with CdS—with the effect being supposedly more pronounced for the VB than for the CB. As a result, the derived VBO and CBO values would need to be considered upper bounds for the real offsets. However, considering that the Cd−Se interface layer most likely will not possess optoelectronic *bulk* properties, the band-gap energy might be significantly larger than the reported bulk E_g of ≈1.7 eV.[38,39] In fact, E_g values exceeding that of bulk CdS have been reported for CdSe quantum dots with diameters smaller than approximately 2 nm,[40] which is larger than the derived interface region where Cd−Se bonds are formed (see above). Thus, we speculate that the resulting band-gap increase might (partially) counterbalance the expected VBM and CBM shifts toward E_F when going from CdS to CdSe resulting in a minor/negligible impact on the derived VBO and CBO offsets at the CdS/CZTSSe interface.

In order to check how this finding correlates with device characteristics, the solar cell manufactured based on the 4 min CdS/CZTSSe sample was studied by $I(V,T)$ measurements. Figure 6 shows the derived V_{OC} as a function of temperature. A linear extrapolation of the open circuit voltages to 0 K is used to derive the activation energy for the dominant recombination process[41] to be E_a = 1.09 ± 0.07 eV. Note that the given comparatively large error interval is due to the increased 0 K extrapolation uncertainty caused by the fact that V_{oc} data are

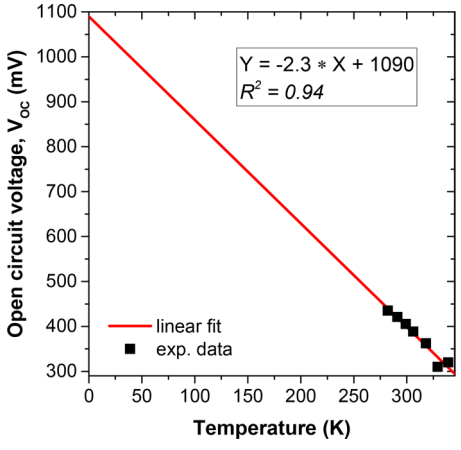

Figure 6. Open circuit voltages as a function of temperature for a solar cell based on a 4 min CdS/CZTSSe sample. The red line indicates the linear extrapolation to 0 K.

only available in a somewhat limited temperature range. However, the comparison with the interface band gap ($E_{g,i}$ = $E_{g,CZTSSe}^{surf}$ + CBO = 1.14 + 0.21 eV = 1.35 eV) representing the energetic barrier for a (high-rate) charge carrier recombination process across the (defect-rich) buffer/absorber interface and the CZTSSe bulk band gap (1.07 eV) representing the barrier for a (low-rate) recombination in the (comparatively defect-poor) absorber bulk allows one to tentatively locate the dominant recombination path. The fact that E_a is significantly lower than $E_{g,i}$ (1.35 eV) but in very good agreement with $E_{g,CZTSSe}$ (1.07 eV), we interpret as indication that the dominant charge carrier recombination in CdS/CTSSe-based solar cells is located in the absorber bulk. Thus, we conclude that the performance of respective devices is not limited by interface recombination. This contradicts the finding that E_a is often reported to be smaller than $E_{g,CZTSSe}$[1,11,12] interpreted as an indication for high-rate recombination at the (buffer/absorber) interface. The pronounced S/(S + Se) profile that has been found for the CZTSSe absorbers of our study (see above) might be an explanation for this deviation.

The derived CBO of 0.21 ± 0.28 eV is significantly smaller than the CBO of 0.56 eV reported by Nagai et al.[42] for the CdS/CZTSe interface but is larger than the −0.3 eV we found for the CdS/CZTS interface.[43] According to device simulations for chalcopyrite-based solar cells,[44−46] the CBO spike of 0.56 eV at the CdS/CZTSe interface would represent a significant barrier for charge carrier transport limiting short circuit current while the −0.3 eV VBO cliff at the CdS/CZTS interface would decrease the energetic barrier for charge carrier recombination opening a high-rate recombination path across the buffer/absorber interface limiting open circuit voltage. Only the CBO 0.21 ± 0.28 eV for the here studied CdS/CZTSSe samples represents an almost ideal electronic interface structure that allows for unimpeded electron transport across the buffer/absorber interface[44−46] while ensuring that the full energetic barrier preventing interfacial charge carrier recombination is established.[17,19] This might explain why kesterite-based solar cells reach highest efficiencies for mixed S/Se compositions.[8] In order to make use of the CBO reduction apparently induced by incorporation of S into the kesterite absorber, only a minor amount of sulfur is required at the kesterite surface. Note that the S/(S + Se) content at the surface of the here studied CZTSSe absorber is below the XPS detection limit of approximately 0.01 (see discussion above and the SI). Based on the higher S/(S + Se) content in the world record device of around 0.25,[8] it can be speculated that even a smaller CB spike or an aligned CB level alignment prevails at the CdS/CZTSSe interface, which would represent the perfect electronic interface structure. Together with the fact that—similar to the here studied devices—also for CdS/CZTSe[11] and low-band-gap CZTSSe[18] solar cells (but *not* for high-band-gap CdS/CZTSSe[1,11,12] and CdS/CZTS[1,13−15] devices) E_a values have been reported that agree with the respective absorber bulk-band-gap energies, we conclude that both the energy level alignment at the CdS/kesterite interface and the charge carrier recombination mechanism critically depend on the S/(S + Se) kesterite composition.

CONCLUSIONS

We studied the interface formation of CdS on low-band-gap CZTSSe thin-film solar cell absorbers by means of characterizing a CdS thickness (deposition time) series by direct and inverse photoemission. In addition, the dominant charge carrier

DOI: 10.1021/acsaem.7b00071
ACS Appl. Energy Mater. 2018, 1, 475−482

recombination mechanism in respective solar cells was investigated by $I(V,T)$ measurements. We find the CZTSSe surface to be completely free of any significant amount of sulfur. Furthermore, Cd−Se bonds are found to be formed at the CdS/CZTSSe interface. The electronic surface band gap of the bare CZTSSe absorber, $E_{g,CZTSSe}^{surf}$, was derived to be 1.14 ± 0.22 eV in agreement with the observed significant Cu deficiency at the kesterite surface. At the CdS/CZTSSe interface a small positive ("spike"-like) conduction band offset of 0.21 ± 0.28 eV was determined. Together with the fact that the resulting interface band gap (1.35 eV) was significantly larger than the $I(V,T)$-derived activation energy of the dominant charge carrier recombination mechanism of 1.09 ± 0.07 eV—which was in excellent agreement with the CZTSSe bulk band gap of 1.07 eV—revealed that the performance of related solar cells is not limited by interface recombination. The latter rather takes place in the (comparatively defect-poor) absorber bulk, and thus the CdS/low-band-gap CZTSSe heterojunction structure is—at least for kesterites with similar S/(S + Se) composition—not responsible for the recent stagnation in performance improvements as it (principally) should allow for high power conversion efficiencies. As a conclusion, the underlying reason for the present open circuit voltage deficiency of kesterite-based solar cells has to be of a different nature. Possible culprits that are discussed include the presence of (harmful) secondary phases,[2−4] the instability of the kesterite/Mo back-contact[3,4] and/or the band-gap narrowing caused by Cu/Zn disorder-induced band tailing.[4,10]

■ ASSOCIATED CONTENT

Supporting Information

The Supporting Information is available free of charge on the ACS Publications website at DOI: 10.1021/acsaem.7b00071.

Current−voltage curves and external quantum efficiency data of related solar cells, XPS signal intensity evolution, and comparison of S 2p spectra of the studied CZTSSe and of a S-free kesterite absorber (PDF)

■ AUTHOR INFORMATION

Corresponding Author

*E-mail: marcus.baer@helmholtz-berlin.de.

ORCID

Marcus Bär: 0000-0001-8581-0691

Norbert Koch: 0000-0002-6042-6447

Notes

The authors declare no competing financial interest.

■ ACKNOWLEDGMENTS

We thank the European Union's Horizon 2020 research and innovation program (Grant Agreement No. 640868) for partial funding. M.B., J.-H.A., and R.G.W. acknowledge additional funding through the Impuls- und Vernetzungsfonds of the Helmholtz Association (Grant No. VH-NG-423). Furthermore, financial support from the MatSEC graduate school of the HZB in cooperation with the Dahlem Research School is gratefully acknowledged by J.-H.A.

■ REFERENCES

(1) Mitzi, D. B.; Gunawan, O.; Todorov, T. K.; Wang, K.; Guha, S. The Path towards a High-performance Solution-processed Kesterite Solar Cell. *Sol. Energy Mater. Sol. Cells* **2011**, *95*, 1421−1436.

(2) Siebentritt, S.; Schorr, S. Kesterites − A Challenging Material for Solar Cells. *Prog. Photovoltaics* **2012**, *20*, 512−519.

(3) Polizzotti, A.; Repins, I. L.; Noufi, R.; Wei, S.-H.; Mitzi, D. B. The State and Future Prospects of Kesterite Photovoltaics. *Energy Environ. Sci.* **2013**, *6*, 3171−3182.

(4) Liu, X.; Feng, Y.; Cui, H.; Liu, F.; Hao, X.; Conibeer, G.; Mitzi, D. B.; Green, M. The Current Status and Future Prospects of Kesterite Solar Cells: A Brief Review. *Prog. Photovoltaics* **2016**, *24*, 879−898.

(5) Persson, C. Electronic and Optical Properties of Cu_2ZnSnS_4 and $Cu_2ZnSnSe_4$. *J. Appl. Phys.* **2010**, *107*, 053710.

(6) Chen, S.; Gong, X. G.; Walsh, A.; Wei, S.-H. Crystal and Electronic Band Structure of Cu_2ZnSnX_4 (X = S and Se) Photovoltaic Absorbers: First-principles Insights. *Appl. Phys. Lett.* **2009**, *94*, 041903.

(7) Paier, J.; Asahi, R.; Nagoya, A.; Kresse, G. Cu_2ZnSnS_4 as a Potential Photovoltaic Material: A Hybrid Hartree-Fock Density Functional Theory Study. *Phys. Rev. B: Condens. Matter Mater. Phys.* **2009**, *79*, 115126.

(8) Wang, W.; Winkler, M. T.; Gunawan, O.; Gokmen, T.; Todorov, T. K.; Zhu, Y.; Mitzi, D. B. Device Characteristics of CZTSSe Thin-Film Solar Cells with 12.6% Efficiency. *Adv. Energy Mater.* **2014**, *4*, 1301465.

(9) See "Inorganic cells (CZTSSe)" power conversion efficiency evolution on the NREL Efficiency Chart (https://www.nrel.gov/pv/assets/images/efficiency-chart.png), showing no improvement after 2014.

(10) Bourdais, S.; Choné, C.; Delatouche, B.; Jacob, A.; Larramona, G.; Moisan, C.; Lafond, A.; Donatini, F.; Rey, G.; Siebentritt, S.; Walsh, A.; Dennler, G. Is the Cu/Zn Disorder the Main Culprit for the Voltage Deficit in Kesterite Solar Cells? *Adv. Energy Mater.* **2016**, *6*, 1502276.

(11) Redinger, A.; Mousel, M.; Wolter, M. H.; Valle, N.; Siebentritt, S. Influence of S/Se Ratio on Series Resistance and on Dominant Recombination Pathway in $Cu_2ZnSn(SSe)_4$ thin film solar cells. *Thin Solid Films* **2013**, *535*, 291−295.

(12) Gunawan, O.; Todorov, T. K.; Mitzi, D. B. Loss Mechanisms in Hydrazine-processed $Cu_2ZnSn(Se,S)_4$ Solar Cells. *Appl. Phys. Lett.* **2010**, *97*, 233506.

(13) Danilson, M.; Kask, E.; Pokharel, N.; Grossberg, M.; Kauk-Kuusik, M.; Varema, T.; Krustok, J. Temperature Dependent Current Transport Properties in Cu_2ZnSnS_4 Solar Cells. *Thin Solid Films* **2015**, *582*, 162−165.

(14) Platzer-Björkman, C.; Frisk, C.; Larsen, J. K.; Ericson, T.; Li, S.-J.; Scragg, J. J. S.; Keller, J.; Larsson, F.; Törndahl, T. Reduced Interface Recombination in Cu_2ZnSnS_4 Solar Cells with Atomic Layer Deposition $Zn_{1-x}Sn_xO_y$ buffer layers. *Appl. Phys. Lett.* **2015**, *107*, 243904.

(15) Wang, K.; Gunawan, O.; Todorov, T.; Shin, B.; Chey, S. J.; Bojarczuk, N. A.; Mitzi, D.; Guha, S. Thermally Evaporated Cu_2ZnSnS_4 Solar Cells. *Appl. Phys. Lett.* **2010**, *97*, 143508.

(16) Turcu, M.; Pakma, O.; Rau, U. Interdependence of Absorber Composition and Recombination Mechanism in $Cu(In,Ga)(Se,S)_2$ Heterojunction Solar Cells. *Appl. Phys. Lett.* **2002**, *80*, 2598.

(17) Scheer, R. Activation Energy of Heterojunction Diode Currents in the Limit of Interface Recombination. *J. Appl. Phys.* **2009**, *105*, 104505.

(18) Krustok, J.; Josepson, R.; Danilson, M.; Meissner, D. Temperature Dependence of $Cu_2ZnSn(Se_xS_{1-x})_4$ Monograin Solar Cells. *Sol. Energy* **2010**, *84*, 379−383.

(19) Klenk, R. Characterisation and Modelling of Chalcopyrite Solar Cells. *Thin Solid Films* **2001**, *387*, 135−140.

(20) Schnabel, T.; Loew, M.; Ahlswede, E. Vacuum-free Preparation of 7.5% Efficient $Cu_2ZnSn(S,Se)_4$ Solar Cells Based on Metal Salt Precursors. *Sol. Energy Mater. Sol. Cells* **2013**, *117*, 324−328.

(21) Schnabel, T.; Abzieher, T.; Friedlmeier, T. M.; Ahlswede, E. Solution-Based Preparation of $Cu_2ZnSn(S,Se)_4$ for Solar Cells—Comparison of $SnSe_2$ and Elemental Se as Chalcogen Source. *IEEE Journal of Photovoltaics* **2015**, *5*, 670−675.

(22) Briggs, D.; Seah, M. P. *Practical Surface Analysis: Auger and X-Ray Photoelectron Spectroscopy*; Wiley: New York, 1990; Vol. *1*, Appendix 1.
(23) Bär, M.; Repins, I.; Weinhardt, L.; Alsmeier, J.-H.; Pookpanratana, S.; Blum, M.; Yang, W.; Heske, C.; Wilks, R. G.; Noufi, R. Zn−Se−Cd−S Interlayer Formation at the CdS/$Cu_2ZnSnSe_4$ Thin-film Solar Cell Interface. *ACS Energy Lett.* **2017**, *2*, 1632.
(24) Inelastic electron mean free paths (IMFP) calculated from the TPP-2M formula: Tougaard, S. *QUASES-IMFP-TPP2M*, Ver. 3.0; QUASES-Tougaard: Odense, Denmark, 2016.
(25) Tanuma, S.; Powell, C. J.; Penn, D. R. Calculations of Electron Inelastic Mean Free Paths. V. Data for 14 Organic Compounds over the 50−2000 eV Range. *Surf. Interface Anal.* **1994**, *21*, 165−176.
(26) Shinotsuka, H.; Tanuma, S.; Powell, C. J.; Penn, D. R. Calculations of Electron Inelastic Mean Free Paths. X. Data for 41 Elemental Solids over the 50 eV to 200 keV Range with the Relativistic Full Penn Algorithm. *Surf. Interface Anal.* **2015**, *47*, 871−888.
(27) Scofield, J. H. Hartree-Slater Subshell Photoionization Cross-section at 1254 and 1487 eV. *J. Electron Spectrosc. Relat. Phenom.* **1976**, *8*, 129−137.
(28) Bär, M.; Schubert, B.-A.; Marsen, B.; Krause, S.; Pookpanratana, S.; Unold, T.; Weinhardt, L.; Heske, C.; Schock, H.-W. Impact of KCN Etching on the Chemical and Electronic Surface Structure of Cu_2ZnSnS_4 Thin-film Solar Cell Absorbers. *Appl. Phys. Lett.* **2011**, *99*, 152111.
(29) *NIST X-ray Photoelectron Spectroscopy Database*, Version 4.1; National Institute of Standards and Technology: Gaithersburg, MD, USA, 2012; http://srdata.nist.gov/xps/.
(30) Wagner, C. D. Auger Lines in X-ray Photoelectron Spectrometry. *Anal. Chem.* **1972**, *44*, 967.
(31) Moulder, J. F. M.; Stickle, W. F.; Sobol, P. E.; Bomben, K. D. *Handbook of X-ray Photoelectron Spectroscopy*; Physical Electronics Division, Perkin-Elmer: Eden Prairie, MN, USA, 1992.
(32) Bär, M.; Lehmann, S.; Rusu, M.; Grimm, A.; Kötschau, I.; Lauermann, I.; Pistor, P.; Sokoll, S.; Schedel-Niedrig, T.; Lux-Steiner, M. C.; Fischer, C.-H.; Weinhardt, L.; Heske, C.; Jung, C. Cd^{2+}/NH_3 − Treatment Induced Formation of a CdSe Surface Layer on $CuGaSe_2$ Thin-Film Solar Cell Absorbers. *Appl. Phys. Lett.* **2005**, *86*, 222107.
(33) Kylner, A.; Lindgren, J.; Stolt, A. Impurities in Chemical Bath Deposited CdS Films for $Cu(In,Ga)Se_2$ Solar Cells and Their Stability. *J. Electrochem. Soc.* **1996**, *143*, 2662−2669.
(34) Enríquez, J. P.; Mathew, X. Influence of the Thickness on Structural, Optical, and Electrical Properties of Chemical Bath Deposited CdS Thin Films. *Sol. Energy Mater. Sol. Cells* **2003**, *76*, 313−322.
(35) Lang, M.; Renz, T.; Mathes, N.; Neuwirth, M.; Schnabel, T.; Kalt, H.; Hetterich, M. Influence of the Cu Content in $Cu_2ZnSn(S,Se)_4$ Solar Cell Absorbers on Order-Disorder Related Band Gap Changes. *Appl. Phys. Lett.* **2016**, *109*, 142103.
(36) Steiner, D.; Dorfs, D.; Banin, U.; Della Sala, F.; Manna, L.; Millo, O. Determination of Band Offsets in Heterostructured Colloidal Nanorods Using Scanning Tunneling Spectroscopy. *Nano Lett.* **2008**, *8*, 2954−2958.
(37) Wei, S.-H.; Zhang, S. B.; Zunger, A. First-principles Calculation of Band Offsets, Optical Bowing, and Defects In CdS, CdSe, CdTe, and their Alloys. *J. Appl. Phys.* **2000**, *87*, 1304−1311.
(38) Shan, W.; Walukiewicz, W.; Ager, J. W.; Yu, K. M.; Wu, J.; Haller, E. E. Pressure Dependence of the Fundamental Band-gap Energy of CdSe. *Appl. Phys. Lett.* **2004**, *84*, 67−69.
(39) Patidar, D.; Rathore, K. S.; Saxena, N. S.; Sharma, K.; Sharma, T. P. Energy Band Gap and Conductivity Measurement of CdSe Thin Films. *Chalcogenide Lett.* **2008**, *5*, 21−25.
(40) Norris, D. J.; Bawendi, M. G. Measurement and Assignment of the Size-dependent Optical Spectrum in CdSe Quantum Dots. *Phys. Rev. B: Condens. Matter Mater. Phys.* **1996**, *53*, 16338−16346.
(41) Nadenau, V.; Rau, U.; Jasenek, A.; Schock, H. W. Electronic properties of CuGaSe2-based heterojunction solar cells. Part I: Transport analysis. *J. Appl. Phys.* **2000**, *87*, 584−593.
(42) Nagai, T.; Udaka, Y.; Takaki, S.; Isowaki, K.; Kawamura, S.; Kawasaki, K.; Tampo, H.; Kim, K. M.; Kim, S.; Shibata, H.; Matsubara, K.; Niki, s.; Terada, N. Electronic Structures of $Cu_2ZnSnSe_4$ Surface and $CdS/Cu_2ZnSnSe_4$ Heterointerface. *Jpn. J. Appl. Phys.* **2017**, *56*, 065701.
(43) Bär, M.; Schubert, B.-A.; Marsen, B.; Wilks, R. G.; Pookpanratana, S.; Blum, M.; Krause, S.; Unold, T.; Yang, W.; Weinhardt, L.; Heske, C.; Schock, H.-W. Cliff-like Conduction Band Offset and KCN-induced Recombination Barrier Enhancement at the CdS/Cu_2ZnSnS_4 Thin-film Solar Cell Heterojunction. *Appl. Phys. Lett.* **2011**, *99*, 222105.
(44) Niemegeers, A.; Burgelman, M.; de Vos, A. On the CdS/$CuInSe_2$ Conduction Band Discontinuity. *Appl. Phys. Lett.* **1995**, *67*, 843−845.
(45) Liu, X.; Sites, J. R. Calculated Effect of Conduction-band Offset on $CuInSe_2$ Solar-cell Performance. *AIP Conf. Proc.* **1996**, *353*, 444−452.
(46) Minemoto, T.; Matsui, T.; Takakura, H.; Hamakawa, Y.; Negami, T.; Hashimoto, Y.; Uenoyama, T.; Kitagawa, M. Theoretical Analysis of the Effect of Conduction Band Offset of Window/CIS Layers on Performance of CIS Solar Cells Using Device Simulation. *Sol. Energy Mater. Sol. Cells* **2001**, *67*, 83−88.

DOI: 10.1021/acsaem.7b00071
ACS Appl. Energy Mater. 2018, 1, 475−482